Chinese Chemical Letters 36 (2025) 110032

Contents lists available at ScienceDirect

Chinese Chemical Letters

journal homepage: www.elsevier.com/locate/cclet

Decomposable and sono-enzyme co-triggered poly(sonosensitizers) for precise and hypotoxic sonodynamic therapy

Shuxin Liu[a], Jinjuan Ma[b], Aiguo Wang[b], Nan Zheng[a,*]

[a] School of Chemical Engineering, Cancer Hospital of Dalian University of Technology, Dalian University of Technology, Dalian 116023, China
[b] Department of Comparative Medicine Laboratory Animal Center, Dalian Medical University, Dalian 116000, China

ARTICLE INFO

Article history:
Received 28 March 2024
Revised 15 May 2024
Accepted 20 May 2024
Available online 21 May 2024

Keywords:
"AND gate" logic
Hypotoxic sonodynamic therapy
Ultrasound and enzyme co-trigger
Sulfate radicals
Förster resonance energy transfer effect

ABSTRACT

A decomposable and sono-enzyme co-triggered nanoparticle (pTCP-CR NP) with "AND gate" logic was synthesized, combining a *meso*–carboxyl-porphyrin-based sonosensitizer (5,10,15,20-tetrakis(carboxyl)porphyrin, TCP) and a thiophenyl-croconium (2,5-bis[(2-(2-(2-hydroxyethoxy)ethoxy)ethyl-4-carboxylate-piperidylamino)thiophenyl]-croconium, CR) *via* ester groups. TCP releases carbon monoxide (CO) under ultrasound (US) irradiation, offering both sonodynamic and gas therapy. CR decomposes into stronger reactive oxygen species (ROS) compared to oxygen-based radicals. The Förster resonance energy transfer (FRET) effect between TCP and CR inhibits ROS and CO generation until triggered by tumor cell overexpressed carboxylesterase (CEs). pTCP-CR NPs "AND gate" logic ensures activation only in the presence of both CEs and US, targeting tumor cells while safety in normal tissues. The ROS and CO generation abilities, as well as the releasing of $SO_4^{\bullet-}$ have been systemically examined. pTCP-CR can be thoroughly decomposed into low-toxic molecules post the treatment, showing the safety with negligible phototoxic reactions. *In vivo* anti-cancer therapy has been evaluated using mice bearing hepatocellular carcinoma.

Precise tumor targeting and on-demand drug release show great potentials in cancer therapy, which have been achieved by the continuously emerging smart prodrugs activated by the specific stimuli [1]. Most of the reported activatable prodrugs (>80%) are sensitive to a single trigger, including the tumor microenvironments (TMEs) like pH [2], glutathione (GSH) [3,4], reactive oxygen species (ROS) [5,6] and enzyme [7], or the external triggers like light, ultrasound, heat, and magnetic field [8,9]. However, in most of the cases, the nonspecific drug accumulation or activation in normal tissues is inevitable because some TMEs are not "specific" enough to sensitively differentiate tumor and normal tissues [10]. Applying "logic gate" involving multiple triggers into the molecular structures can remarkably magnify the specific tumor targeting and attenuate the undesired toxicity *via* the introduction of multi-stage "locks" and sophisticating the "unlock" conditions [11]. More than two stimuli co-govern the "on and off" of the drug, exhibiting "OR gate" or "AND gate" features [12]. Most of the reported prodrugs with logic gates are "OR gates", that is, drugs can be partially activated by either stimulus [13,14]. Even though sometimes the tumor targeting and anti-cancer efficacy can be magnified upon the combination of multiple stimuli, the partial activation feature of the "OR gate" determines the toxicity induced by single stimulus cannot be thoroughly avoided [15]. Compared to "OR gate", "AND gate" endows the prodrug with the "only" activation upon the co-existence of all the stimuli [16,17], which was first reported in the design of a boron dipyrromethene responsive to both Na^+ and H^+ ions by Akkaya [18]. However, due to the molecule synthesis and design challenging, the "AND gate" is infrequent among numerous prodrugs.

Among the stimuli, a combination of external stimulus and internal stimulus owns advanced strengths due to the tumor-specific and spatio-temporal control features. Ultrasound (US) as a mechanical force has been applied into the cancer treatment as an external stimulus, called sonodynamic therapy (SDT) [19]. Sonosensitizers bearing macrocyclic structures like porphyrin and phthalocyanine, can be activated under low-intensity US irradiation to produce highly toxic ROS through the sonoluminescence mechanism [20,21]. Compared to other treatments, SDT owns the advantages of spatio-temporal control, noninvasiveness, minor energy attenuation, and deep tissue-penetration [22,23]. However, the US-triggered "AND gate" prodrug has been rarely reported due to the following challenges. First, unlike the pro-chemodrug which the drug activation is based on the transformation or exposure of spe-

* Corresponding author.
E-mail address: nzheng@dlut.edu.cn (N. Zheng).

https://doi.org/10.1016/j.cclet.2024.110032
1001-8417/

cific functional groups upon the triggers, it is hard to inhibit the sonosensitizers' toxicity upon US trigger *via* simple change of functional groups [24,25]. As the toxicity of sonosensitizers is mainly originated from the US's energy and sonoluminescence, Förster resonance energy transfer (FRET) effect which has been widely applied in the design of dyes, is a promising strategy to suppress the toxicity from the "only" US irradiation [26]. Second, killing of the tumor cells for SDT greatly relies on the ROS (singlet oxygen ($^1O_2$) and oxygen-based radicals ($^{\bullet}OH$)) produced by the US-irradiated sonosensitizers. Limited by the tolerate dosage and intracellular uptake level of the sonosensitizers, as well as the oxidative ability and life time of the ROS, the anticancer efficacy for SDT cannot reach as good as that for chemotherapy or radiotherapy [27,28]. Therefore, stronger ROS agents or toxic agents are extremely needed to boost the cytotoxicity.

Considering the above-mentioned two issues in the design of "AND gate" SDT prodrugs, we specially design two monomers including a *meso*–carboxyl-porphyrin-based sonosensitizer (5,10,15,20-tetrakis(carboxyl)porphyrin, TCP) and a croconium (thiophenyl-croconium (2,5-bis[(2-(2-(2-hydroxyethoxy)ethoxy) ethyl-4-carboxylate-piperidylamino)thiophenyl]-croconium, CR), as well as their polymers (pTCP-CR) to solve all the listed obstacles in a US and enzyme co-activated system. 5,10,15,20-Tetrakis(carboxyl)porphyrin (TCP) was selected since it can release ROS and carbon monoxide (CO) with US irradiation [29]. To further improve the toxicity of the ROS generated by SDT, sulfate radicals ($SO_4^{\bullet-}$) with stronger oxidation capability are introduced into the molecule design. $SO_4^{\bullet-}$ has an oxidation potential of 2.5–3.1 eV, which is similar to that of $^{\bullet}OH$ (2.80 eV), but the half-life ($SO_4^{\bullet-}$, 30 μs) is 30 times *versus* $^{\bullet}OH$, which means that it has stronger cytotoxicity due to longer diffusion distance and leads to more effective oxidation reactions [30]. Recently, it has been revealed that $SO_4^{\bullet-}$ can be produced by sulfate ions (SO_4^{2-}) and $^{\bullet}OH$, which is a mild method appliable in biomedical field [31]. Therefore, a specific CR dye bearing thiophene group is designed as a SO_4^{2-} precursor since sulfur-containing dye owns the potential to release SO_4^{2-} upon ROS treatment [32]. Third, the absorbance of the CR usually covers the emission of most porphyrin-based sonosensitizers upon US irradiation. Thus, CR can act as a quencher to lock the undesired US-induced ROS generated due to the FRET effect once it is connected with porphyrin *via* suitable linkers [26].

With the features of *meso*–carboxyl porphyrin and thiophene-croconium at hand, TCP and CR are designed and polymerized into a polymeric prodrug (pTCP-CR) with cross-linked network structure *via* ester linkers (Scheme 1). Through self-assembly in water, it is prepared into nanoparticles (pTCP-CR NPs) (Scheme S2 in Supporting information) [33]. As shown in Scheme 1, activation of pTCP-CR NPs requires the presence of both carboxylesterase (CEs) and US. Under "only CEs" activation, pTCP-CR NPs cleave into TCP and CR monomers with low cytotoxicity. Under "only US" activation, ROS generation by TCP is quenched by CR, and CO generation is blocked by ester linkers. Only with the co-existence of CEs and US, TCP and CR release as monomers, enabling ROS and CO generation. ROS from TCP further decompose CR into SO_4^{2-} and more toxic $SO_4^{\bullet-}$, enhancing cytotoxicity. This enzyme and US co-triggered "AND gate" design enables precise spatio-temporal control over the release of anticancer agents. The efficacy of pTCP-CR NPs as a smart decomposable polysonosensitizer is demonstrated through *in vitro* experiments using cell lines with varying CEs expression levels and *in vivo* SDT efficacy on mice with hepatocellular carcinoma (HCC).

Although the instability and bleachability of squarylium dyes and CR dyes in the presence of metal ions or light have been reported [34], the phenomenon that CR dye can be degraded by ROS and transformed into active agents has not been reported.

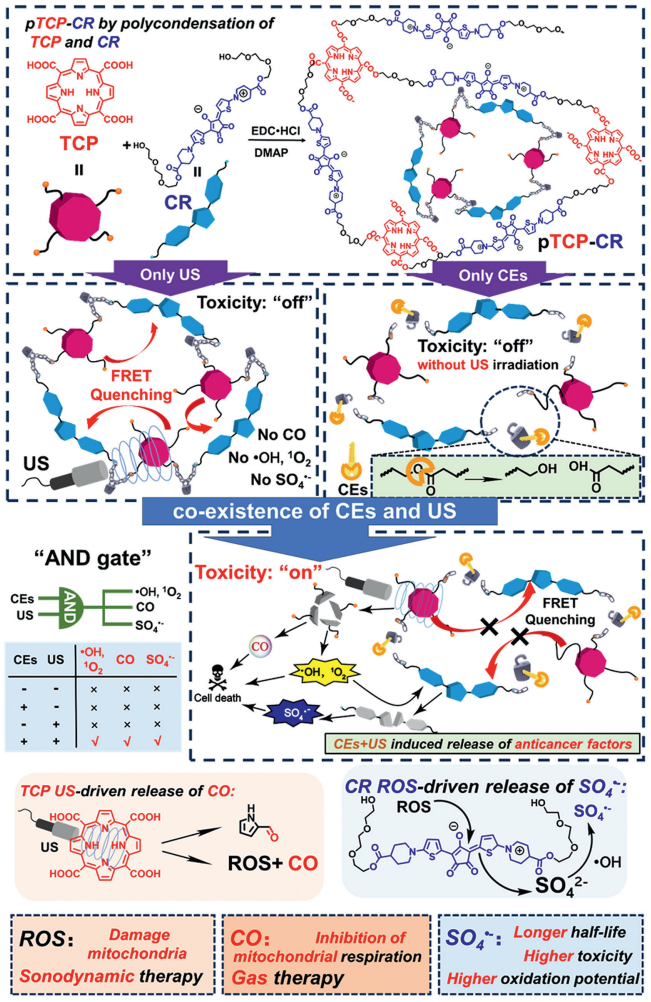

Scheme 1. Schematic illustration of the "AND gate" logic in the design of pTCP-CR NPs for the releasing of CO, ROS and $SO_4^{\bullet-}$ under the co-triggers of US and CEs.

As sulfur-containing dyes owned the potentials to be converted to SO_4^{2-} after being treated by ROS [32], CR bearing thiophenol group was selected as the special monomer for the releasing of surfur-based radicals. CR was synthesized by the nucleophilic substitution, alkali saponification/acid hydrolysis, condensation processes with croconic acid as shown in Scheme S2. All the intermediates and finally compounds were fully characterized (Figs. S1–S8 in Supporting information). It has been demonstrated before that US could trigger the porphyrin derivatives to generate $^{\bullet}OH$, similar with the porphyrin-based photodynamic therapy mechanism [35]. We then evaluated whether the ROS generated by the US and TCP would lead to the decomposition of CR into SO_4^{2-} as well as more active $SO_4^{\bullet-}$ radicals (Fig. 1a). Adding $^{\bullet}OH$ to a phosphate buffer saline (PBS) solution of CR led to a significant reduction in CR absorption in the near-infrared (NIR) region (around 700 nm) (Fig. 1b). ^1H nuclear magnetic resonance spectroscopy (^1H NMR) and high resolution mass spectrometry (HRMS) analyses confirmed CR decomposition after $^{\bullet}OH$ treatment for 20 and 50 min, with CR molecules breaking down into low molecular weight compounds (Figs. S9 and S10 in Supporting information). Additionally, we assessed if $^{\bullet}OH$ generated by TCP could decompose CR. As anticipated, CR absorption in the NIR region decreased after US treatment of a mixed solution of TCP and CR in PBS (Fig. S11 in Supporting information), while minimal change occurred in the CR + US group and the CR+TCP group (Fig. S11). This suggested CR decomposition relied on ROS from TCP and US combina-

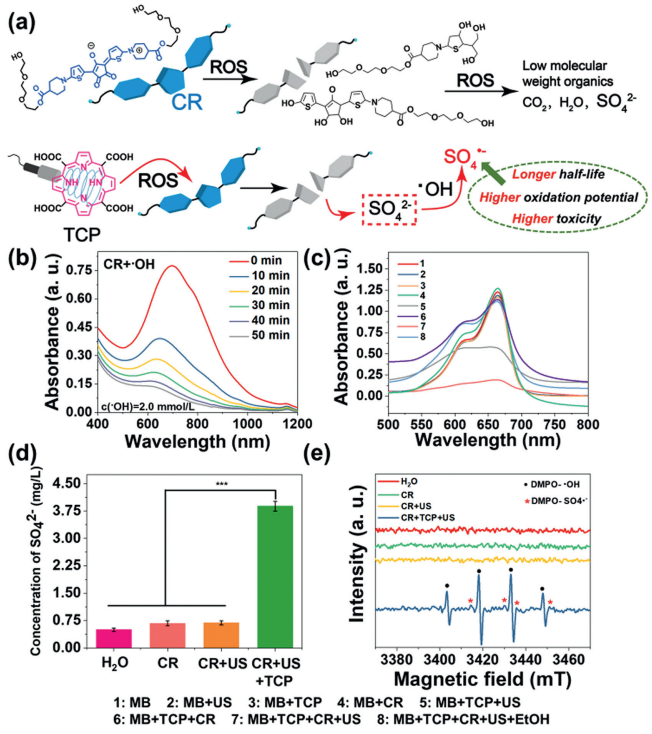

Fig. 1. (a) The ROS-induced CR decomposition and release of $SO_4^{\bullet-}$. (b) Absorption spectra of a 50 μmol/L solution of CR after reaction with $^{\bullet}OH$. (c) The degradation efficiency of MB by $^{\bullet}OH$ and $SO_4^{\bullet-}$ produced by different experimental groups. (d) The concentration of SO_4^{2-} in H_2O, CR, CR with US irradiation and CR + TCP with US irradiation. (e) EPR spectra of produced $^{\bullet}OH$ and $SO_4^{\bullet-}$ radicals from H_2O by the CR, CR with US irradiation and CR + TCP with US irradiation. Data are means ± SD ($n = 3$). $^{***}P < 0.001$.

tion. Furthermore, high performance high performance (HPIC) was utilized to determine SO_4^{2-} concentration in various CR solutions (only CR group, CR + US group, CR + TCP + US group, and deionized water group). Results showed a significantly higher SO_4^{2-} concentration in the CR + TCP + US group (3.88 mg/L) compared to control groups (0.5–0.7 mg/L) (Fig. 1d, Fig. S12 and Table S1 in Supporting information).

It has been reported that SO_4^{2-} can be efficiently converted into $SO_4^{\bullet-}$ by $^{\bullet}OH$ [36]. Electron paramagnetic resonance (EPR) analyses were used to examine the $SO_4^{\bullet-}$ radicals that are derived from both CR and TCP under US treatment (Fig. 1a). Obvious sulfate anion (DMPO-$SO_4^{\bullet-}$, labeled by red star) signals were observed only in the CR + TCP + US treatment group (Fig. 1e). The EPR spectra supported that the $^{\bullet}OH$ produced by TCP under US irradiation can effectively convert SO_4^{2-} into $SO_4^{\bullet-}$. Since the degradation of methylene blue (MB) could indirectly reflect the oxidative ability of $^{\bullet}OH$ and $SO_4^{\bullet-}$, the capability of $^{\bullet}OH$ and $SO_4^{\bullet-}$ were compared using different combination of CR, TCP and US [37]. The results indicated that CR can effectively degrade MB in the presence of TCP and US, with up to 84.5% of MB being degraded, indicating that CR can produce $^{\bullet}OH$ and $SO_4^{\bullet-}$ under the combined treatment of TCP and US (Fig. 1c and Fig. S13 in Supporting information).

Considering the advanced features of TCP and CR including the generation of CO, $^1O_2$ and $SO_4^{\bullet-}$, a polymerized TCP and CR (pTCP-CR) with cross-linked network structure connected by flexible ester linkers was designed and synthesized using our previously reported polycondensation method (Scheme S3 in Supporting information) [21,38]. As controls, polymerized TCPP and CR (pTCPP-CR) which could not release CO, and polymerized TCP with hexaethylene glycol (pTCP-HG) which did not generate $SO_4^{\bullet-}$ were also synthesized for comparisons. Their chemical structures were characterized by ^1H NMR spectroscopy (Figs. S14–S16 in Supporting information). Their molecular weights (MWs) were calculated to be around 6900 (pTCP-CR), 9200 (pTCPP-CR) and 6100 (pTCP-HG) g/mol by gel permeation chromatography (GPC) (Fig. S17 in Supporting information). pTCP-CR, pTCPP-CR and pTCP-HG were prepared into nanoparticles (pTCP-CR NPs, pTCPP-CR NPs and pTCP NPs) in PBS by the self-assembly of hydrophilic and hydrophobic units [39,40]. These NPs showed unimodal size distributions with the average hydrodynamic diameters of 79.5 ± 2.8 nm (pTCP-CR NPs), 187.3 ± 3.3 nm (pTCPP-CR NPs) and 232.5 ± 6.2 nm (pTCP-HG NPs) measured by dynamic light scattering (DLS) (Fig. S18 in Supporting information). A spherical morphology of pTCP-CR NPs was observed with scanning electron microscopy (SEM) (Fig. S19 in Supporting information). After co-incubation with CEs (20 U/mL), the size of pTCP-CR NPs increased to over 1000 nm due to ester linker cleavage, causing nanoparticle structure destruction. These NPs contain three anti-cancer agents: CO, $^1O_2$, and $SO_4^{\bullet-}$, making them a prodrug. pTCP-CR NPs degrade into TCP and CR monomers when interacting with cancer cells overexpressing CEs but remain stable against normal tissues with limited CEs expression. TCP's emission (600–750 nm) overlaps with CR's absorption (600–800 nm), enabling the FRET effect (Figs. 2a, c and d) [41]. Therefore, the CR moiety in pTCP-CR NPs structure had the potential to act as a quencher, which would fully quench the fluorescence emission and ROS generation of TCP segment due to the presence of FRET process. However, the FRET effect of pTCP-CR NPs was inhibited in the monomeric state after CEs treatment (Fig. 2c and Figs. S22–S24 in Supporting information). The distance between the energy donor (TCP) and energy acceptor (CR) was an important factor affecting FRET effect [42]. The intermolecular interaction between TCP unit and CR unit is simulated. The intermolecular distance in the polymer mode (<10 Å) is much lower than that in the monomer mode (>15 Å) (Fig. S20 in Supporting information). In addition, due to the cleavage of pTCP-CR NPs by esterase, the change of FRET effect was time-dependent. In the polymer state, all the three active agents including CO, $^1O_2$ and $SO_4^{\bullet-}$ were inactivated due to the quenching effect of CR on TCP.

As a result, all the active agents were double-locked into pTCP-CR NPs, which could be only unlocked by the simultaneous existence of US and CEs (Scheme S4 in Supporting information). As shown in Fig. 2b, pTCP-CR NPs is processed by both US and CEs, both the TCP absorbance at 300–450 nm and CR absorbance at 600–1000 nm dramatically decreased. This indicates that both TCP and CR are decomposed after CEs/US dual processing. As a control, pTCP-CR NPs showed strong stability under only US or CEs irradiation (Fig. S25 in Supporting information). Subsequently, the ROS generation ability of CR, TCP + CR, pTCP-CR NPs and pTCPP-CR NPs in water upon different treatment conditions was evaluated. 1,3-Diphenylisobenzofuran (DPBF) and 2′,7′-dichlorodihyrofluorescein (DCFH) were used as $^1O_2$ and ROS analytical reagent [43]. For CEs/US-co-treated pTCP-CR NPs and pTCPP-CR NPs, the absorption of DPBF (420 nm) decreased significantly with the prolongation of US treatment time, indicating the $^1O_2$ generation upon US irradiation. As controls, if pTCP-CR NPs and pTCPP-CR NPs were only irradiation by US without CEs treatment, the absorption of DPBF did not change and no generation of $^1O_2$ (Fig. S26 in Supporting information). Such results were in consistent with the fluorescence results that FRET effect inhibited the generation of $^1O_2$ from TCP unit. Apart from DPBF, DCFH as a fluorescent probe, was also selected to demonstrate it. Compared with the only US triggered group, CEs/US co-triggered pTCP-CR NPs or pTCPP-CR NPs showed notable stronger fluorescence intensity, revealing the "on and off" of ROS was fully determined by the co-existence of CEs and US (Fig. 2d and Fig. S27 in Supporting information).

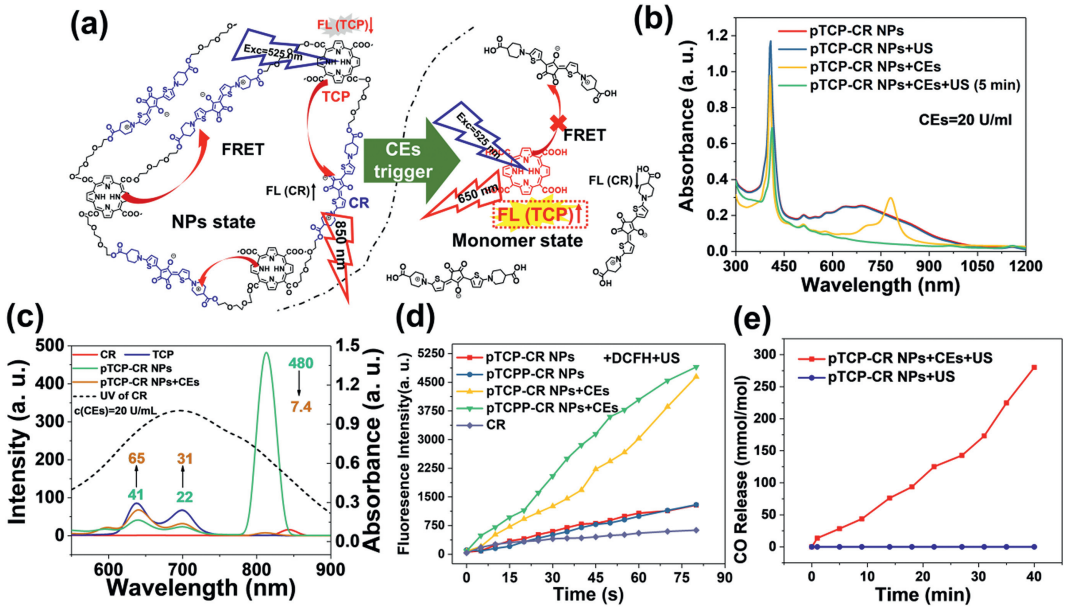

Fig. 2. (a) Schematic illustration of the FRET effect between the TCP and CR. (b) Absorbance intensity change of pTCP-CR NPs in response to 5 min US treatment with or without CEs. (c) Fluorescence spectra and intensity change of CR, TCP, pTCP-CR NPs and pTCP-CR NPs with 20 U/mL CEs in aqueous solution (excitation wavelength: 525 nm) and ultraviolet–visible spectroscopy (UV–vis) spectra of CR in H_2O (black dashed line). (d) Time-dependent fluorescence spectra of DCFH indicating US-induced ROS generation by CR, pTCP-CR NPs, pTCPP-CR NPs, pTCP-CR NPs + CEs and pTCPP-CR NPs + CEs. (e) US trigger CO release of pTCP-CR NPs with and without CEs as a function of time.

The CEs/US co-triggered CO release ability of pTCP-CR NPs was quantified by hemoglobin method, 9-(diethylamino)−5*H*-benzo[*a*]phenoxazin-5-one palladium complex (1-Ac) CO fluorescence probe method and CO gas sensor method. UV spectra indicated conversion of Hb-Fe(II) to Hb-Fe(CO) after incubating CEs-treated pTCP-CR NPs with hemoglobin under US treatment. Fluorescence intensity of CEs-treated pTCP-CR NPs with 1-Ac increased significantly under US treatment, confirming CO release (Fig. S28 in Supporting information). CO gas sensor method quantified CO release at 280 mmol CO/mol TCP after 40 min of US treatment. No CO release was observed in pTCP-CR NPs treated only with US irradiation (Fig. 2e). Similar results were observed with pTCP-HG NPs (Fig. S28). Additionally, SO_4^{2-} release from pTCP-CR NPs under CEs/US dual activation was significantly higher compared to other groups (Fig. S29 in Supporting information). In summary, the co-existence of CEs and US triggered the generation of CO, $^1O_2$, and $SO_4^{\bullet-}$.

Subsequently, we evaluated the *in vitro* release of ROS and CO from the double-blocked pTCP-CR NPs upon CEs/US triggers. It was known that the CEs expression in liver tumors was much higher than normal tissues [44]. CEs-positive hepatoma cells (HepG2) and CEs-negative cells (293T and LO2) were selected as the models to demonstrate the *in vitro* anticancer efficacy [45]. After incubation with pTCP-CR NPs (20 μmol/L porphyrin) for 4 h, bright fluorescence showed internalization in HepG2 cells, confirmed by colocalization with Mito-Tracker Green, indicating effective enrichment in mitochondria (Fig. 3a). Cellular uptake of pTCP-CR NPs was higher than free TCP in both HepG2 and 293T cells, suggesting improved internalization due to NPs formation [46]. Similar results were observed with pTCPP-CR NPs (Fig. S30 in Supporting information).

DCFH-diacetate (DA) and 1-Ac were furthermore used to detect the intracellular ROS and CO. In HepG2 cells, both pTCP-CR NPs and pTCPP-CR NPs showed green fluorescence upon US irradiation, while fluorescence dropped significantly in 293T and LO2 with or without US (Fig. 3a, Figs. S31 and S32 in Supporting information). Sole US treatment did not induce green fluorescence. The US-triggered ROS generation of pTCP-HG NPs was not influenced by cell type, blurring the tumor-normal cell distinction (Fig. S32). Adding CEs inhibitor bis-*p*-nitrophenyl phosphate (BNPP) to HepG2 cells reduced green fluorescence in pTCP-CR NPs + US and pTCPP-CR NPs + US groups, but not in pTCP-HG NPs + US group (Fig. 3b and Fig. S32). This aligns with ROS generation tuned by CEs and US co-existence, targeting toxicity to tumor cells under US. Similarly, intracellular CO release upon US showed CEs/US dependency. HepG2 cells incubated with pTCP-CR NPs and pTCP-HG NPs displayed intracellular CO production after US, evidenced by strong red fluorescence using 1-Ac (Figs. 3c and d, Fig. S33 in Supporting information). No CO was detected in 293T cells or HepG2 cells treated with BNPP. Thus, pTCP-CR NPs specifically generate ROS and CO only with CEs and US co-existence, targeting high CEs tumor cells under US.

The MTT assay evaluated the toxicity of pTCP-CR NPs, pTCPP-CR NPs, and pTCP-HG NPs on cancer cells. All NPs showed low cytotoxicity without US irradiation, indicating their safety (Fig. 3e and Fig. S34 Supporting information). Upon US irradiation, HepG2 cells treated with pTCP-CR NPs and pTCPP-CR NPs exhibited significantly higher cytotoxicity (Fig. 3f and Fig. S35 in Supporting information). Pre-treatment of HepG2 cells with BNPP decreased therapeutic efficiency, consistent with results in cells with limited CEs expression. At 25 μmol/L concentration (porphyrin equivalent), cell mortality was significantly higher in the pTCP-CR NPs + US group (81.37% ± 3.27%) compared to pTCPP-CR NPs + US (59.77% ± 1.35%) due to CO gas therapy from the TCP moiety (Fig. 3f). Additionally, mortality was higher in the pTCP-CR NPs + US group than pTCP-HG NPs + US (64.36% ± 2.25%) due to more efficient oxidative toxicity of $SO_4^{\bullet-}$ from CR (Fig. S36 in Supporting information). These results demonstrate the contribution of both SDT and GT therapy to cell death, activated only by CEs and US. CO and ROS can induce mitochondrial dysfunction and lead to cell apoptosis by decreasing mitochondrial membrane potential (MMP). To assess the therapeutic effect, MMP reduction was measured using 5,5′,6,6′-tetrachloro-1,1′,3,3′-tetraethylbenzimidazolo carbocyanine iodide (JC-1) dye. Following US-triggered treatment, HepG2 cells showed a significant decrease in MMP, shifting JC-1 dye fluorescence from red to green, indicating mitochondrial dysfunction

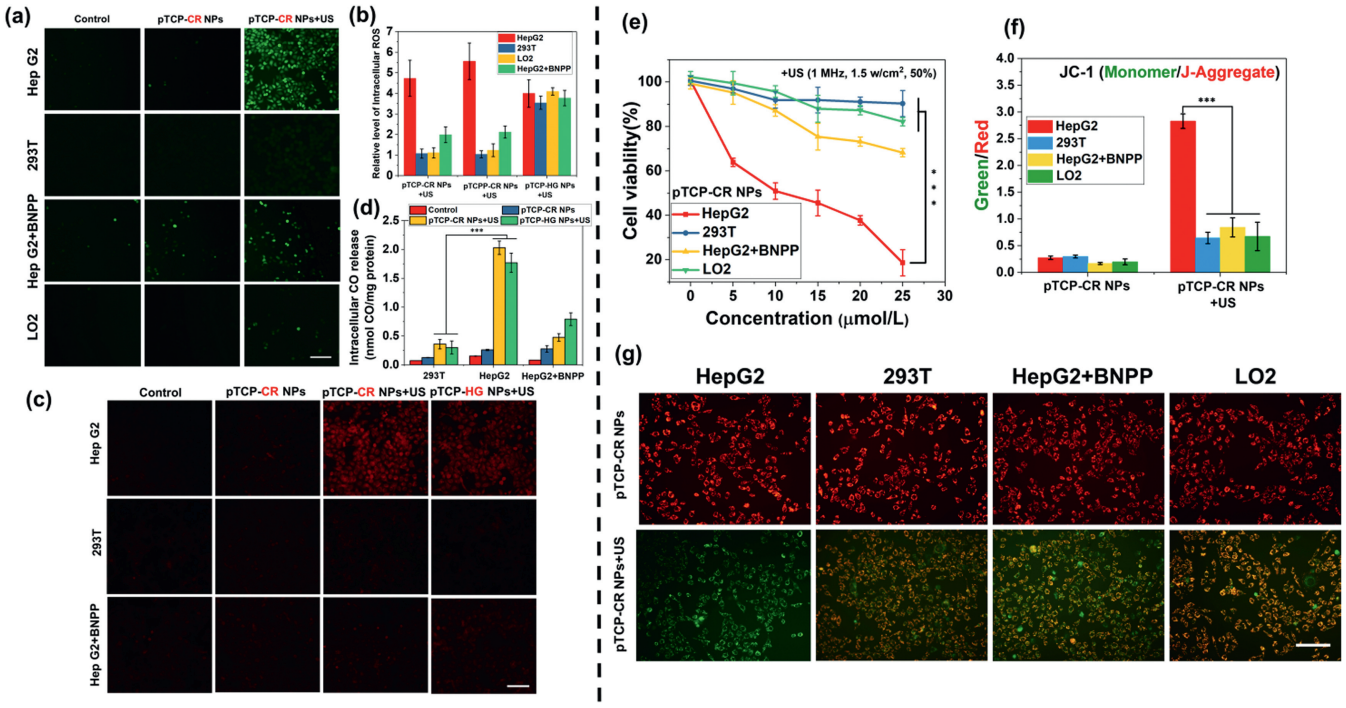

Fig. 3. (a) Fluorescence images of cells with ROS probe DCFH-DA after 4 h of treatment with pTCP-CR NPs with or without US. (b) Intracellular ROS levels in various cells after pTCP-CR NPs, pTCPP-CR NPs, or pTCP-HG NPs with US. (c) CLSM images of cells stained with 1-Ac probe for CO detection after treatment with pTCP-CR NPs and pTCP-HG NPs with US. (d) Intracellular CO release from NPs with and without US in different cells. (e) Cell viabilities of cells incubated with pTCP-CR NPs at varying concentrations with US treatment. (f) Ratio and (g) CLSM images of JC-1 monomer to aggregate in mitochondria after pTCP-CR NPs treatment with or without US. Data are means ± SD ($n = 4$). $^{***}P < 0.001$. Scale bar: 50 μm.

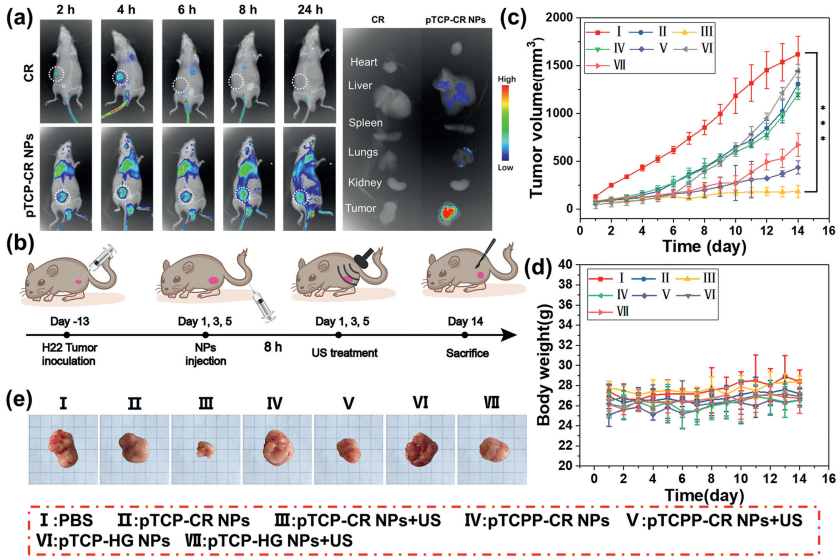

Fig. 4. (a) *In vivo* and *ex vivo* fluorescence images of subcutaneous H22 tumor-bearing mice at different time points (2, 4, 6, 8, and 24 h) post-injection of CR or pTCP-CR NPs (5 mg/kg dose equivalence of CR), with excised organs and tumors at 8 h. (b) Scheme of *in vivo* tumor suppression experiment. (c) Time-dependent tumor-volume curves. (d) Body weight changes. (e) Digital graphs of dissected solid tumors on day 14. All data are means ± SD ($n = 6$). $^{***}P < 0.001$.

(Fig. 3g). The green/red fluorescence intensity ratio, indicative of mitochondrial damage, was highest in HepG2 cells treated with pTCP-CR NPs and US, demonstrating the most effective mitochondrial damage compared to other cell lines (Figs. S36–S38 in Supporting information).

The *in vivo* synergistic anti-cancer therapy was furthermore evaluated using mice bearing H22 tumors. All animal experimental procedures were approved by the Institutional Animal Care and Use Committee (IACUC) of Dalian Medical University. The approval number of animal experiments is AEE22049. Initially, pTCP-CR NPs served as an *in vivo* fluorescence imaging agent to assess drug accumulation and retention. After intravenous injection into mice, fluorescence signals were recorded over time. Results showed discernible signals at the tumor site 2 h post-injection, peaking at 8 h. Minimal signals were observed in mice injected with free CR. Major organs and tumors were harvested 24 h post-injection for *ex vivo* fluorescence imaging (Fig. 4a). We evaluated the combined therapeutic efficacy of pTCP-CR NPs, pTCPP-CR NPs and pTCP-HG NPs in H22 tumor-bearing mice. Mice were divided into seven groups: PBS only, NPs only, NPs with US, with detailed administra-

tion in Fig. 4b, monitoring tumor sizes and body weights daily. Tumors in untreated and NPs-treated mice grew rapidly, while those in groups receiving US showed some inhibition compared to PBS. Notably, group III (pTCP-CR NPs + US) displayed the highest inhibition, releasing both CO and enhanced ROS upon US. Tumor images and hematoxylin-eosin staining (H&E) staining confirmed these findings. Mice treated with NPs and US showed no significant weight loss or organ damage, suggesting safety (Figs. 4c–e, Figs. S39 and S40 in Supporting information).

In summary, a CEs and US co-triggered polysonosensitizer pTCP-CR NPs with "AND gate" logic was developed, in which TCP with ROS and CO generation ability was polymerized with CR with FRET quenching effect and $SO_4^{\bullet-}$ generation capability *via* ester linkers. Either CEs or US itself could not "unlock" pTCP-CR NPs with the releasing of active agents while the anti-cancer efficacy could only be activated upon the co-existence of CEs and US. Such design could avoid the nonspecific targeting and drug activation in the normal tissues *via* the combination of CEs as the internal trigger and US as an external trigger. A spatio-temporal control of the toxicity activation could also be achieved. Upon activation by two triggers, advanced anti-cancer agents beyond traditional ROS from SDT were simultaneously generated due to the smart design of TCP and CR monomers. TCP monomer can not only generate traditional ROS upon US irradiation, but also be decomposed into CO as therapeutic gas. CR monomer can not only quench the toxicity of TCP at polymer state due to FRET effect, but also be decomposed into $SO_4^{\bullet-}$ as more toxic ROS for toxicity boosting. Post SDT treatment, pTCP-CR NPs can be thoroughly decomposed into low-toxic molecules for the fast clearance, avoiding phototoxic side-effect. Such "AND gate" logic design provided a promising strategy for the precise tumor treatment with limited side-effect.

Declaration of competing interest

The authors declare that they have no known competing financial interests or personal relationships that could have appeared to influence the work reported in this paper.

CRediT authorship contribution statement

Shuxin Liu: Writing – review & editing, Writing – original draft, Data curation. **Jinjuan Ma:** Data curation. **Aiguo Wang:** Writing – review & editing, Writing – original draft, Resources. **Nan Zheng:** Writing – review & editing, Writing – original draft, Project administration, Conceptualization.

Acknowledgments

This work was supported by grants from the National Natural Science Foundation of China (No. 22375027), the Natural Science Foundation of Jiangsu Province (Nos. BK20221265, BK20211100), the Fundamental Research Funds for the Central Universities (No. DUT23YG133), and the Research Funds from Liaoning Cancer Hospital (No. 2024ZLKF-35). The authors acknowledge the assistance of DUT Instrumental Analysis Center.

Supplementary materials

Supplementary material associated with this article can be found, in the online version, at doi:10.1016/j.cclet.2024.110032.

References

[1] R.H. Zhang, T.Q. Nie, L.Y. Wang, et al., Biomater. Sci. 11 (2023) 4254–4264.
[2] Y. Zhuang, S. Han, Y. Fang, et al., Coordin. Chem. Rev. 455 (2022) 214360.
[3] Y. Tao, C. Dai, Z. Xie, et al., Chin. Chem. Lett. 35 (2023) 109170.
[4] H. Liu, T. Nie, X. Duan, et al., J. Control. Release 359 (2023) 132–146.
[5] G. Yang, Y. Liu, J. Chen, et al., Acc. Mater. Res. 3 (2022) 1232–1247.
[6] H.Z. He, L.H. Du, M. Tan, et al., Sci. China Chem. 63 (2020) 936–945.
[7] J.H. Xie, S.Y. Tian, H.N. Zhang, et al., Biomacromolecules 24 (2023) 2225–2236.
[8] J. Zhang, J. Yan, Y. Wang, et al., Chin. Chem. Lett. 35 (2024) 108434.
[9] Z. Wang, M. Wang, Y. Qian, et al., Chin. Chem. Lett. 34 (2023) 107853.
[10] H. Wang, Z. Xu, Q. Li, et al., Eng. Regener. 2 (2021) 137–153.
[11] M. Chen, C. Wang, X. Wang, et al., Adv. Mater. 36 (2024) e2307818.
[12] C. Luo, L. He, F.M. Chen, et al., Cell Rep. Phys. Sci. 2 (2021) 100350.
[13] J.T.F. Lau, P.C. Lo, X.J. Jiang, et al., J. Med. Chem. 57 (2014) 4088–4097.
[14] H. Xiong, K.J. Zhou, Y.F. Yan, et al., ACS Appl. Mater. Interface 10 (2018) 16335–16343.
[15] L.G. Tang, Z. Yang, Z.J. Zhou, et al., Theranostics 9 (2019) 1358–1368.
[16] M.Q. Chen, C.H. Wang, Z.X. Ding, et al., ACS Cent. Sci. 8 (2022) 837–844.
[17] C.X. Yan, Z.Q. Guo, Y.J. Liu, et al., Chem. Sci. 9 (2018) 6176–6182.
[18] S. Ozlem, E.U. Akkaya, J. Am. Chem. Soc. 131 (2009) 48–49.
[19] D. Huang, J. Wang, C. Song, et al., Innovation 4 (2023) 100421.
[20] C.T. Deng, M.C. Zheng, S.P. Han, et al., Adv. Funct. Mater. 33 (2023) 2300348.
[21] S.X. Liu, J.J. Ma, E.Y. Xue, et al., Adv. Healthc. Mater. 12 (2023) 2300481.
[22] X.T. Pan, N. Wu, S.Y. Tian, et al., Adv. Funct. Mater. 32 (2022) 2112145.
[23] Y. Zhang, X.Q. Zhang, H.C. Yang, et al., Chem. Soc. Rev. 50 (2021) 11227–11248.
[24] E.G. Kaye, B. Mirabi, I.R. Lopez-Miranda, et al., J. Am. Chem. Soc. 145 (2023) 12518–12531.
[25] G.C. Wang, Y. Su, X.L. Chen, et al., Bioact. Mater. 25 (2023) 189–200.
[26] L.K.B. Tam, J.C.H. Chu, L. He, et al., J. Am. Chem. Soc. 145 (2023) 7361–7375.
[27] S. Son, J.H. Kim, X.W. Wang, et al., Chem. Soc. Rev. 49 (2020) 3244–3261.
[28] S. Liang, X.R. Deng, P.A. Ma, et al., Adv. Mater. 32 (2020) 2003214.
[29] S. Liu, J. Ma, X. Xu, et al., Sci. China Chem. 67 (2024) 1624–1635.
[30] X.D. Duan, X.X. Niu, J. Gao, et al., Curr. Opin. Chem. Eng. 38 (2022) 100867.
[31] C. Agarkoti, A. Chaturvedi, P.R. Gogate, et al., Sep. Purif. Technol. 312 (2023) 123351.
[32] X.J. Yu, J. Zhang, Y.Y. Chen, et al., J. Environ. Chem. Eng. 9 (2021) 106161.
[33] T. Nie, H. Liu, Z. Fang, et al., ACS Nano 17 (2023) 10925–10937.
[34] M. Tian, S. Tatsuura, M. Furuki, et al., J. Am. Chem. Soc. 125 (2003) 348–349.
[35] Z. Zhou, T. Wang, T.T. Hu, et al., Mater. Chem. Front. 7 (2023) 1684–1693.
[36] T. Li, Y.M. Chen, X.M. Wang, et al., Appl. Catal. B: Environ. 285 (2021) 119830.
[37] S.M. Wu, P. Wang, J.W. Qin, et al., Adv. Funct. Mater. 31 (2021) 2102160.
[38] N. Zheng, Z.Y. Zhang, J. Kuang, et al., ACS Appl. Mater. Interface 11 (2019) 18224–18232.
[39] Z. Sun, Y. Hou, BMEMat 1 (2023) e12012.
[40] W.C.W. Chan, BME Front. 4 (2023) 0016.
[41] M.C. Dos Santos, W.R. Algar, I.L. Medintz, et al., Trends Anal. Chem. 125 (2020) 115819.
[42] J. Qian, H.N. Cui, X.T. Lu, et al., Chem. Eng. J. 401 (2020) 126017.
[43] T. Entradas, S. Waldron, M. Volk, J. Photoch. Photobiol. B: Biol. 204 (2020) 111787.
[44] K. Na, M. Kim, C.Y. Kim, et al., J. Proteome. Res. 19 (2020) 4867–4883.
[45] J.J. Tan, Z.Y. Deng, C.Z. Song, et al., J. Am. Chem. Soc. 143 (2021) 13738–13748.
[46] J.J. Chen, Z.Y. Jiang, Y.S. Zhang, et al., Appl. Phys. Rev. 8 (2021) 041321.